Journal of Power Sources 245 (2014) 801–807

Contents lists available at SciVerse ScienceDirect

Journal of Power Sources

journal homepage: www.elsevier.com/locate/jpowsour

Nitrogen-doped graphene prepared by a transfer doping approach for the oxygen reduction reaction application

Zaiyong Mo [a,b], Ruiping Zheng [a], Hongliang Peng [a], Huagen Liang [a], Shijun Liao [a,*]

[a] The Key Laboratory of Fuel Cell Technology of Guangdong Province & The Key Laboratory of New Energy, School of Chemistry and Chemical Engineering, South China University of Technology, Guangzhou 510641, China
[b] School of Chemistry and Chemical Engineering, Zhao Qing University, Guangdong, Zhao Qing 526061, China

HIGHLIGHTS

- Nitrogen doped graphene catalyst is prepared by a facile transfer doping approach.
- The nitrogen content of the catalyst is high up to 6.25 at%.
- This catalyst shows ORR catalytic activity comparable to Pt/C in alkaline medium.

GRAPHICAL ABSTRACT

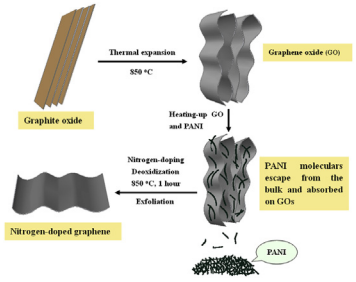

ARTICLE INFO

Article history:
Received 23 April 2013
Received in revised form
25 June 2013
Accepted 7 July 2013
Available online 16 July 2013

Keywords:
Graphene
Nitrogen-doped
Polyaniline
Oxygen reduction reaction

ABSTRACT

Well defined nitrogen-doped graphene (NG) is prepared by a transfer doping approach, in which the graphene oxide (GO) is deoxidized and nitrogen doped by the vaporized polyaniline, and the GO is prepared by a thermal expansion method from graphite oxide. The content of doped nitrogen in the doped graphene is high up to 6.25 at% by the results of elements analysis, and oxygen content is lowered to 5.17 at%. As a non-precious metal cathode electrocatalyst, the NG catalyst exhibits excellent activity toward the oxygen reduction reaction, as well as excellent tolerance toward methanol. In 0.1 M KOH solution, its onset potential, half-wave potential and limiting current density for the oxygen reduction reaction reach 0.98 V (vs. RHE), 0.87 V (vs. RHE) and 5.38 mA cm^{-2}, respectively, which are comparable to those of commercial 20 wt% Pt/C catalyst. The well defined graphene structure of the catalyst is revealed clearly by HRTEM and Raman spectra. It is suggested that the nitrogen-doping and large surface area of the NG sheets give the main contribution to the high ORR catalytic activity.

1. Introduction

Graphene has attracted great attention owing to its exceptional physical, chemical, and mechanical properties, as well as its promising application ranging from micro-electronics to energy-storage [1–4]. Recently, it is found that the modified graphene could be used as efficient electrocatalysts [5–10], or super-capacitors [11–13]. In particular, it is significant to use modified graphene as cathode catalysts of fuel cell for facilitating the oxygen reduction reaction (ORR), which is the key electrode reaction occurring at the cathode of fuel cell. Up to now, Pt/C based electrocatalysts are the most popular catalysts used to catalyze ORR for their high intrinsic catalytic activity [14–17]. However, due to their high cost, scarcity, and poor tolerance to the methanol, etc, Pt/C based catalysts remain the greatest obstacle to large-scale commercialization of fuel cells [18]. Therefore, developing inexpensive non-Pt catalysts with high ORR activity and good methanol tolerance has driven much of the applied and fundamental fuel cell researches in recent years [19–27].

* Corresponding author. Tel./fax: +86 20 87113586.
E-mail address: chsjliao@scut.edu.cn (S. Liao).

0378-7753/$ – see front matter © 2013 Elsevier B.V. All rights reserved.
http://dx.doi.org/10.1016/j.jpowsour.2013.07.038

Among all the non-Pt catalysts, the modified graphenes have been regarded as a potential category owing to their unique features derived from the monolayer of carbon atoms. Recently, the graphenes modified by transition metal oxide [28–31] or doped by hetero atoms [32,33] with satisfying performance toward the ORR have been demonstrated. Liang et al. [34,35] obtained well dispersed cobalt oxide and manganese-cobalt oxide on the graphene through a hydrothermal reaction and investigated their electrocatalytic activity toward ORR in alkaline media. These new materials were found to possess excellent electrocatalytic activity and stability. Lin et al. [36] synthesized nitrogen-doped graphene via pyrolysis of graphene oxide and urea, the N content reached to 7.86 at%. This graphene catalyst exhibited excellent ORR activity, showing onset potential of −0.1 V in oxygen saturated 0.1 M KOH solution, as well as good durability and tolerance of the methanol. Wang et al. [37] developed a facile approach to prepare a graphene catalyst doped with both N and B. This co-doped graphene exhibited superior electrocatalytic activity toward ORR, durability, anti-CO poison and tolerance of the methanol to the commercial 20 wt% Pt/C catalyst. The results of First-principles calculation revealed that the substitution of C by heteroatoms led to smaller energy gap between the highest-occupied molecular orbital and the lowest-unoccupied molecular orbital, and then resulted in higher ORR catalytic activity. Besides, graphene co-doped with N and S reported by Liang [38] and Yang [39] showed fairly good ORR catalytic activity. Moreover, heat-treated hemin supported on graphene nanoplatelets was also found to have excellent ORR catalytic activity [40].

Recently, polyaniline (PANI) was used as a precursor to prepare nitrogen-doped carbon material with excellent ORR catalytic activity [41–44]. In our earlier experiments on nitrogen-doped carbon material derive from PANI used as non-Pt ORR catalyst [45], it is found that the PANI is movable in the quartz tube during its pyrolysis in the furnace. Inspired by this phenomenon, we attempted to prepared nitrogen-doped graphene (NG) by a transfer doping method, making graphene oxide (GO) reduced and nitrogen doped by the pyrolysis of polyaniline vaporized from a polyaniline containing boat put below the GO containing boat. As expected, this NG catalyst has fine nanosheet morphology and exhibits excellent ORR catalytic activity comparable to commercial Pt/C catalyst in alkaline media.

2. Experimental

2.1. Materials preparation

Graphite oxide was prepared from 10,000 mesh graphite powder using a modified hummers' method [28,35,46], and the graphene oxide (GO) sample was prepared by a thermal expansion approach, in which the graphite oxide powder was thermally expanded in a tubular furnace at 850 °C and Ar atmosphere for 30 min.

Polyaniline was synthesized via the previously reported chemical oxidation polymerization method [43,45], using aniline and ammonium persulfate as monomer and oxidant, respectively. The polymerization was carried out in 0.5 M HCl aqueous solution at 0–10 °C for 24 h.

Nitrogen-doped graphene was prepared by a transfer doping method. As in details, a PANI containing quartz boat is covered by a GO containing boat mentioned above, and putting them in a tubular furnace with Ar flow, the deoxidation and doping of GO were proceeded by increasing the temperature to 850 °C at the rate of 20 °C min^{-1}, and then keeping the temperature at 850 °C for 60 min.

2.2. Characterization

The SEM was conducted with a Nova Nano Scanning Electron Microscope 430 (Quantum Design, USA) operated at 30 kV. The TEM observation was performed with a JEM-2100 Transmission Electron Microscope (JEOL, Japan) operated at 120 kV. XRD was conducted on a TD-3500 powder diffractometer (Tongda, China) operated at 40 kV and 30 mA, using Cu-Kα as radiation sources. XPS was performed on a VG ESCALAB MK2 X-ray photoelectron spectrometer (VG, England) operated at 12.5 kV and 250 W, using Al-Kα as radiation source. Raman spectra were recorded on a Lab RAM Aramis Raman Spectrometer (HJY, France) with the spectrum range from 1000 to 3000 cm^{-1}, using 532 nm laser as spectrum source. The functional groups in the material were characterized by a Fourier transform infrared (FTIR) spectroscopy (Shimadzu, Japan) with the wave number resolution of 4 cm^{-1} in the range from 1800 to 100 cm^{-1}. The bulk nitrogen content measurement was conducted on a Vario EL cube elemental analyzer (Elementar, Germany). Specific surface areas were measured with a nitrogen adsorption–desorption method on a Tristar II 3020 gas adsorption analyzer (Micromeritics, USA).

The atomic N/C and O/C ratios were calculated from the XPS line intensities (I) using the approximate relationships [47]:

$$\frac{n_i}{n_j} = \frac{I_i}{I_j} \times \frac{\sigma_j}{\sigma_i} \times \frac{E_{k_j}^{0.5}}{E_{k_i}^{0.5}} \quad (1)$$

$$E_k = h\nu - E_b \quad (2)$$

where n_i is the atomic number of element i. I_i is the XPS intensity of element i, using the peak area. σ_i is the cross-section of element i (C1s = 1.00, N1s = 1.80, O1s = 2.93) [48]. Ek_i is the kinetic energy, for Al-Kα radiation source, $h\nu$ = 1486.6 eV. E_b is the binding energy of element i. The quantitative data are reported in Table 1.

2.3. Electrocatalytic evaluation

Voltammetry tests were carried out on an electrochemical workstation (Ivium, Netherlands) at room temperature, using a three-electrode configuration. Ag/AgCl (3 M NaCl) was used as the reference electrode, and a platinum foil was used as the counter electrode. The work electrode was prepared using the following procedures: 10 mg catalyst was dispersed ultrasonically in 1 ml Nafion/ethanol (0.25 wt. % Nafion) for 30 min, then 5 μL of the dispersion was transferred and spread on a glassy carbon substrate electrode (5 mm inner diameter) by a micropipette, followed by drying under an infrared bulb. The cyclic voltammetry (CV) and linear sweep voltammetry (LSV) were performed in 0.1 M KOH aqueous solution with rotation speed of zero and 1600 rpm respectively, the sweeping rate is 10 mV s^{-1}. All the LSV data is not corrected for the N_2-data. All potentials in this paper are referenced to a reversible hydrogen electrode (RHE), and the potential difference between RHE and Ag/AgCl electrode in the alkaline electrolyte is 0.99 V.

Table 1
The surface and bulk compositions of NG sample measured by XPS and elemental analysis.

Characterizing method	Nitrogen content (at%)	Carbon content (at%)	Sulfur content (at%)	Oxygen content (at%)
XPS	6.27	90.23	0	3.50
Elemental analysis	6.25	87.16	1.89	4.70

3. Results and discussion

3.1. Morphology and structure

Fig. 1 shows the SEM images of the as-prepared unexfoliated GOs. From the sectional view in Fig. 1a, it can be observed that the GO sheets prepared by thermal expansion of graphite oxide overlap loosely over each other, and each sheet exhibits a zigzag shape along the border with the two adjacent sheets at both sides, demonstrating the layers of graphite can be efficiently separated via the oxidation using modified hummer's method followed by thermal expansion process. Fig. 1b shows the top view of the unexfoliated GOs, a large GO sheet with some folds can be seen. It could be expected that the interconnected GOs can be divided into isolated GO sheets by ultrasonic exfoliation.

Fig. 2 displays a typical TEM image of an isolated NG sheet with ca. 1.5 μm width obtained from ultrasonic exfoliation of the deoxidized and nitrogen-doped GO. The crumply surface verifies the typical morphology of graphene.

As shown in Fig. 3a, the FTIR spectra reflect the functional groups of NG and GO clearly. In the spectrum of GO sample, the peaks at ca. 1734, 1597,1400 and 1123 cm^{-1} could be attributed to the bond moisture in C═O, C═C, O–H and C–C, respectively [36,37,49,50]. The strong feature band at 1458 cm^{-1} derives from $-CH_3$. Another feature band at 1169 cm^{-1} is corresponding to C–O–C [49]. All the band information confirms the characteristic of GO. However, for NG sample, some characteristic bands corresponding to GO disappeared, implying the occurrence of deoxidization (or reduction) of GO in the pyrolysis process [51]. The disappearance of band at 1458 cm^{-1} can be ascribed to $-CH_3$ decomposed at high temperature for 1 h. It is noteworthy that the band of C═C has a blue shift from 1597 to 1636 cm^{-1}, it may be related with the disappearance of C═O at 1734 cm^{-1} and nitrogen-doping. Moreover [52], a new emerged peak at ca. 1545 cm^{-1} is the characteristic peak of C═N bond [53], an indication that nitrogen has been doped in the graphene. As shown in Fig. 3a, it is clearly that the FTIR spectrum of NG is almost same to that of N_xC (carbonization of PANI), but much different from that of GO, further demonstrating the doping of nitrogen to the graphene.

Fig. 3b shows the Raman spectra of GO and NG. The D band and G band locating at around 1348 cm^{-1} and 1586 cm^{-1} are observed. The G band arises from the bond stretching of sp^2-bonded pairs, including C–C, C–N, while the D band is corresponding to the sp^3 defect sites, including vacancy and hetero atoms. Although there is no significant change in the position of D and G bands, NG shows a larger I_D/I_G value than that of GO (1.08 vs. 1.00), owing to the introduction of defects by nitrogen-doping. The stronger 2D peaks

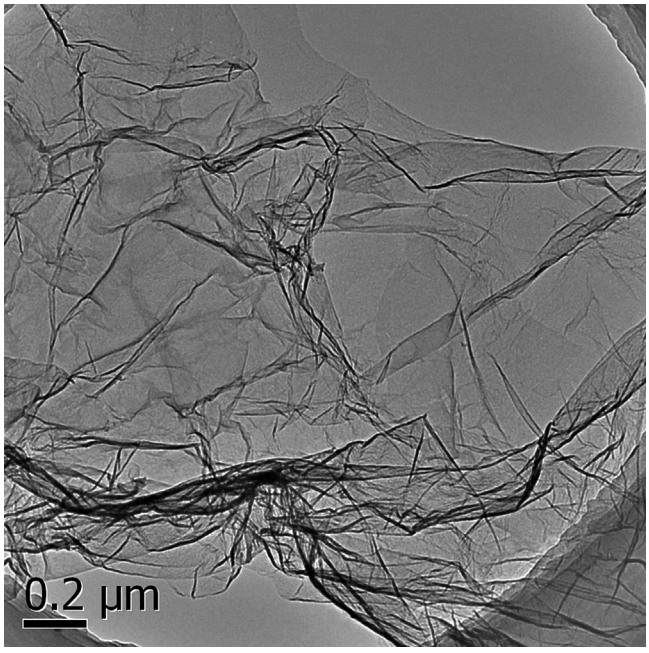

Fig. 2. TEM image of nitrogen-doped graphene sheet.

($\sim$2688 cm^{-1}) and the more readily visible defect-activated $D + D'$ peaks ($\sim$2913 cm^{-1}) are the other indications of defects [37,54]. The overall band intensity of NG is higher than that of GO, suggesting the loss of carbon in GO lattice, possibly caused by the strong oxidation of modified hummers' method in the preparation of graphite oxide, is somewhat made up by the pyrolyzing process.

As compared in Fig. 4, both GO and NG exhibit different XRD patterns from nitrogen doped carbon black (N_xC), showing asymmetrical diffraction peaks corresponding to C (002) at 2θ near 25°. For both GO and NG samples, this peak shifts to lower angle slightly, and seems split into two peaks, However, the shape and strength of two peaks for both samples are quite different, for NG, the higher peak appears at higher angle, but the higher peak appears at lower angle for GO sample. Indicating the slightly structure changes were occurred after deoxidation and N-doping. Furthermore, the intensities of C(002) and C(101) of both GO and NG are much weaker than that of N_xC [55], it is generally considered as an important feature of graphene materials containing few number of layers [56].

By the BET measurement results, the surface areas of sample NG is high up to 1119 $m^2\ g^{-1}$, 4.7 times of that of sample N_xC

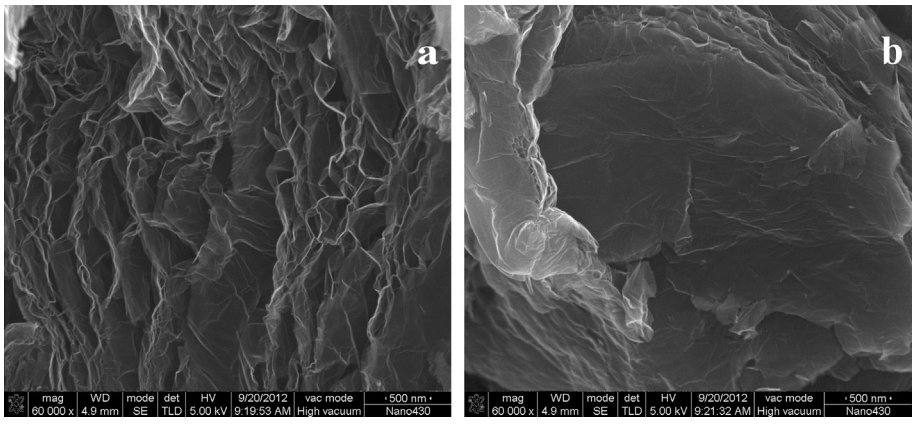

Fig. 1. SEM image of GO sample at sectional view (a); and top view (b).

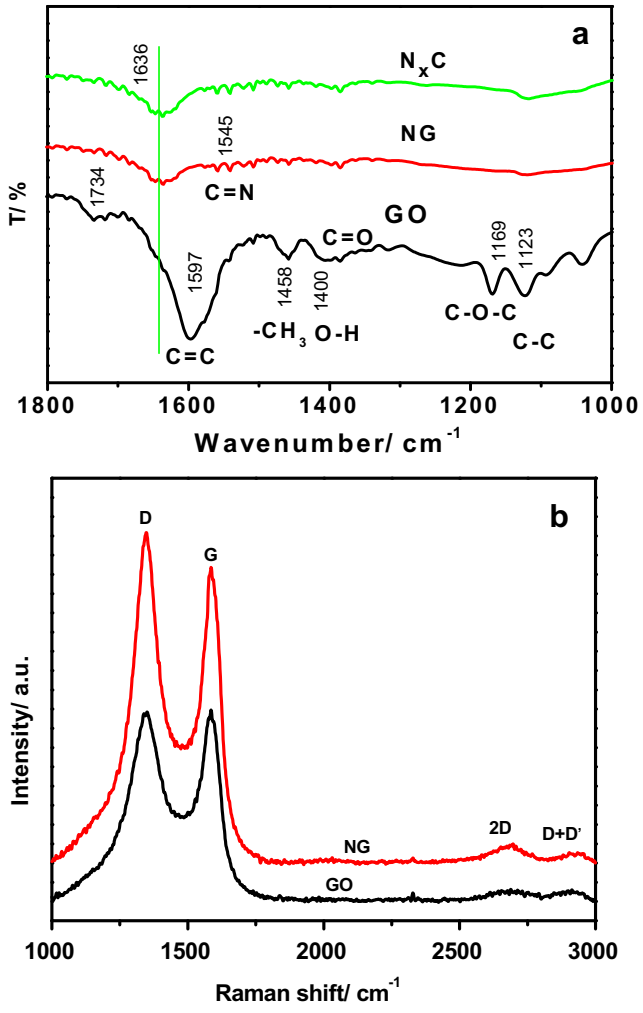

Fig. 3. FTIR spectra of GO, NG and N_xC (a); Raman spectra of GO and NG (b).

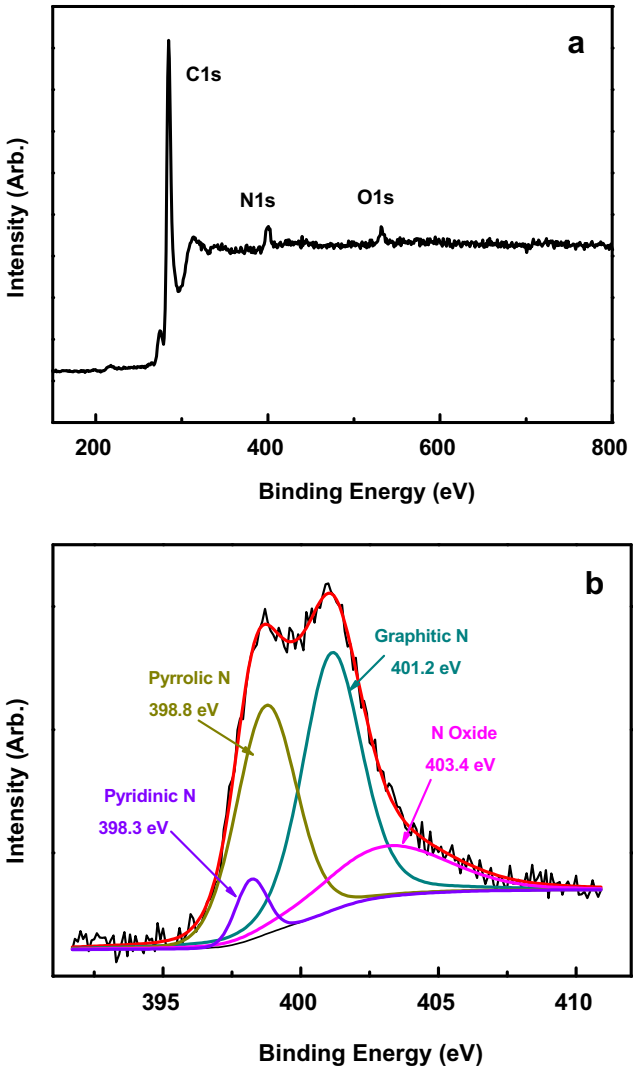

Fig. 5. Survey XPS spectrum of NG (a); High-resolution N1s XPS spectrum of NG and fitted curves of different types of nitrogen (b).

(238 $m^2\ g^{-1}$), confirming the good graphene structure with few monolayers of NG sample.

Fig. 5a shows the XPS survey data of the material. It reveals that the NG is composed mainly of carbon (C1s = 284.8 eV), oxygen (O1s = 532.9 eV), nitrogen (N1s = 401.0 eV). The quantitative data are reported in Table 1. The surface composition calculated from XPS data reveals that the contents of nitrogen, carbon and oxygen are 6.27, 90.23 and 3.50 at%, respectively; these compositions are quite consistent with the bulk compositions measured with the elemental analysis (Table 1). It is worth to note that the content of nitrogen at surface is almost same to the bulk nitrogen, implying that during the process of pyrolysis, along with the temperature rising, the PANI molecules or clusters escaping from the bulk precursor are not only adsorbed on the surface of GO clusters, but also penetrate the interior of the GO sheets to make the whole sheets nitrogen doped.

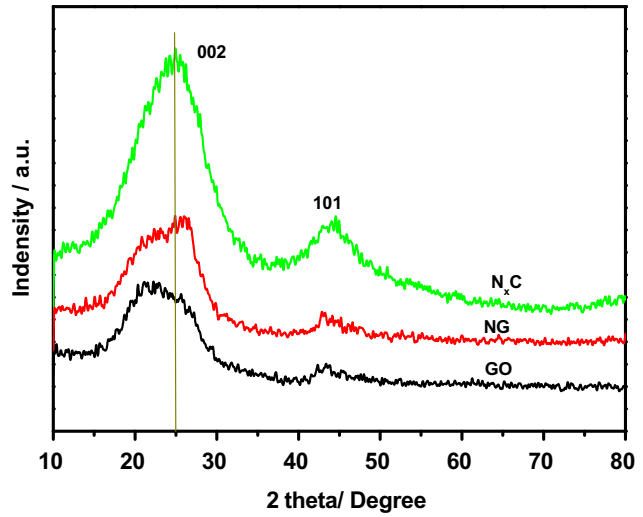

Fig. 4. XRD patterns of GO, NG and N_xC.

According to the elemental analysis results, the sulfur content in the NG sample is ca. 1.89 at%, however, there is no detectable S2p peak at 164.0 eV in the XPS survey spectra, we assume that although a few of sulfur derived from ammonium persulfate in PANI exists in the NG sample, the majority of sulfur may exist in the interior instead of the exterior of the nano-sheets, the result is that the surface content almost undetectable by XPS.

Fig. 5b displays the high-resolution N1s XPS spectrum of the NG sample, as well as the fitted spectra of different types of nitrogen moiety probably existing in the sample fitted with the

Lorentzian–Gaussian multi-peak fit technique. The asymmetric N1s spectrum indicates the existence of four types of nitrogen moiety: pyridinic nitrogen at 398.3 eV [57], pyrrolic nitrogen at 398.8 eV [53], graphitic nitrogen at 401.2 eV [39], and nitrogen oxide at 403.4 eV [58,59]. It can be confirmed by the results of XPS that nitrogen could be doped into the graphene via the transfer doping approach.

3.2. Electrocatalytic activity for ORR

The CV curves for NG in N_2- and O_2-saturated 0.1 M KOH aqueous solution are presented in Fig. 6a. In N_2-saturated electrolyte, except for a clear capacitive CV, no visible peak can be observed, indicating no oxygen (from solution phase) reduction reaction occurs. On the contrary, when the CV is conducted in O_2-saturated KOH solution, besides the capacitive CV background, a well-defined oxygen reduction peak at 0.86 V with 1.1 mA cm^{-2} maximal current density is obtained, implying that this non-Pt catalyst possesses excellent ORR catalytic activity in the alkaline electrolyte.

Fig. 6b presents the ORR polarization curves for GO, N_xC, NG and 20 wt. % commercial Pt/C (JM) in O_2-saturated 0.1 M KOH solution. The GO shows poor activity toward the ORR, while N_xC presents higher activity than GO owing to its N-doping; however, the NG sample shows excellent ORR activity, which is comparable with the commercial Pt/C. The onset potential of NG reaches up to 0.98 V, positively shifting 110 mV and 60 mV from that of GO and N_xC, indicating that the process of transfer pyrolysis can make the GO deoxidized and doped with nitrogen effectively, and then endows the NG excellent ORR catalytic activity. The large surface area of NG sample is another factor for its high ORR activity.

As shown in Fig. 6b, all the three parameters associated to ORR activity, onset potential, half-wave potential and limiting current density of NG are almost the same to those of commercial 20 wt% Pt/C, implying this non-precious metal catalyst is already comparable to the commercial Pt/C (JM) in alkaline electrolyte.

It should be pointed out that there is a peak at the junction of the mixed kinetics-diffusion control region and diffusion-controlled region in the ORR plot of NG, and with the increasing of the electrode rotation rate, this peak weakens gradually (Fig. 7a). This phenomenon may be owing to the less efficient oxygen diffusion, which results from the slow electrolyte flow in the holes built by overlapping NG sheets. With the increase of the electrode rotation rate, faster electrolyte flow results in efficient oxygen diffusion, and then weaker peak.

To investigate the kinetics of the ORR on NG catalyst, we measured the ORR curves at various rotating rates of electrode as shown in Fig. 7a, and a series of the Koutecky–Levich plots (i^{-1} vs. $\omega^{-1/2}$) derived from Fig. 7a are obtained. It is clearly that the K–L plots present good linearity (Fig. 7b), and the slopes remain approximately constant over the potential range from 0.85 to

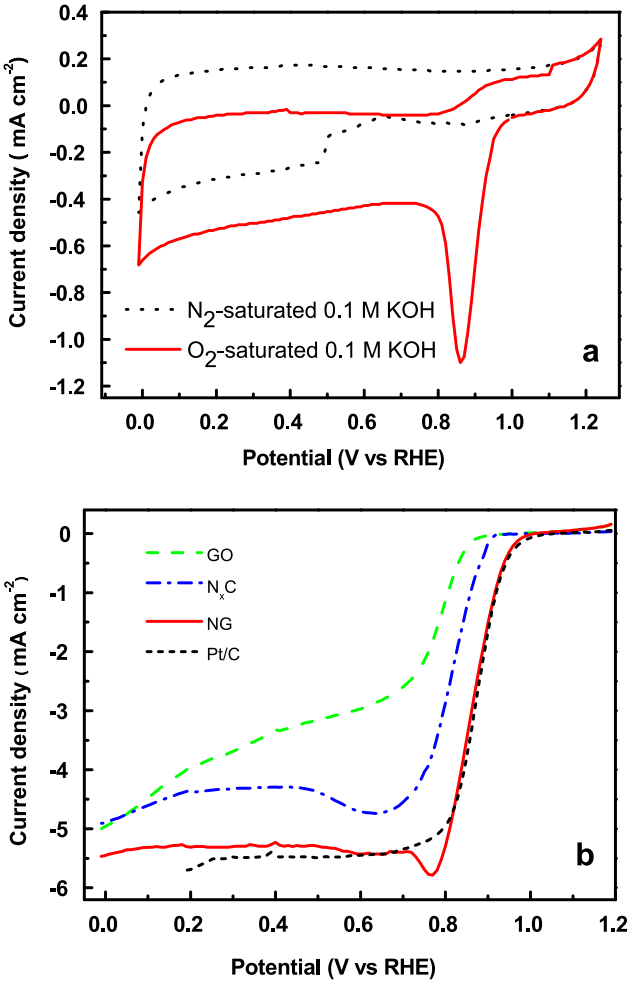

Fig. 6. CV spectra of NG catalyst in N_2-saturated and O_2-saturated 0.1 M KOH with zero rotation rate (a); ORR curves of GO, NG and 20 wt.% Pt/C catalysts in O_2-saturated 0.1 M KOH with disk rotating rate of 1600 rpm (b).

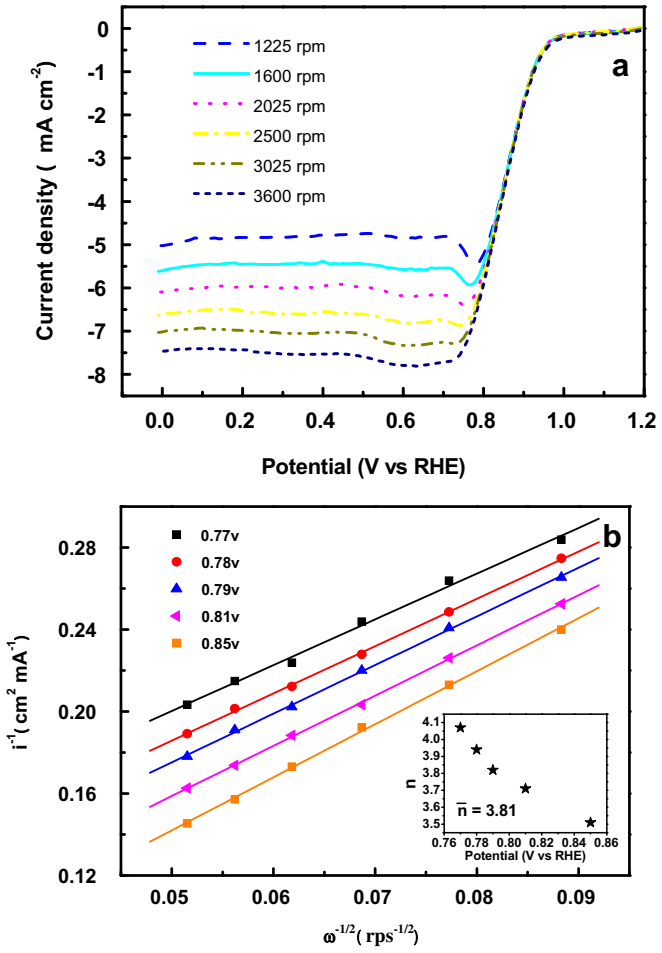

Fig. 7. ORR curves of NG catalysts obtained at different rotating rates (a); *K–L* plots of current density reciprocal versus $\omega^{-1/2}$ at different potential on NG electrode (b).

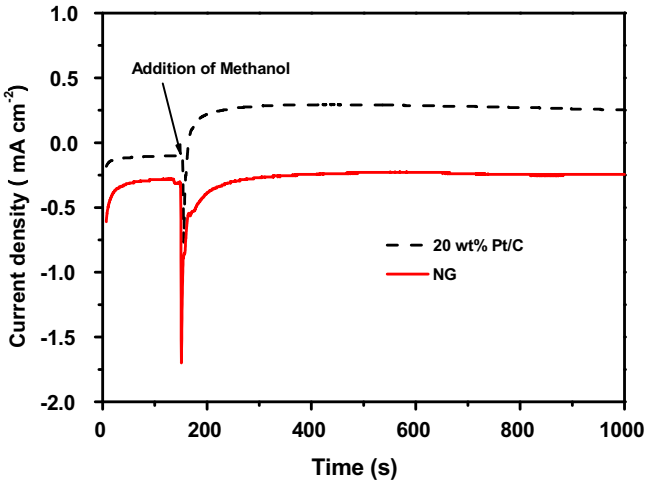

Fig. 8. Chronoamperometric response of NG and Pt/C catalysts at −0.25 V in O_2-saturated 0.1 M KOH with 10% (w/w) methanol.

0.77 V, suggesting the similar transferred electron number for ORR at different potentials. The transferred electron number (n) per molecule of oxygen involved could be calculated based on the Koutecky–Levich Eq. (3),

$$i^{-1} = i_k^{-1} + \left(0.62nFCD^{2/3}\gamma^{1/6}\omega^{1/2}\right)^{-1} \quad (3)$$

where i is the measured current density, i_k is the kinetic current density, n is the number of electrons transferred during the ORR, F is the Faraday constant ($F = 96{,}485$ C mol^{-1}), C is the bulk concentration of O_2 ($C = 1.2 \times 10^{-3}$ mol L^{-1}), D is the diffusion coefficient of O_2 in the 0.1 M KOH electrolyte ($D = 1.9 \times 10^{-5}$ cm^2 s^{-1}), γ is the kinetic viscosity of the electrolyte ($\gamma = 0.01$ cm^2 s^{-1}), and ω is the angular velocity of the disk ($\omega = 2\pi N$, N is the linear rotation rate) [60]. The dependence of n on the potential in the case of NG electrode is shown as an inset in Fig. 6b. The average n value is 3.81, very close to 4, it reveals that the ORR on the NG catalyst follows the 4 electrons transfer pathway.

For practical applications, tolerance to the methanol is an important consideration for the cathode catalyst of direct methanol fuel cells. Fig. 8 exhibits the chronoamperometric responses of static NG and Pt/C electrodes measured at 0.74 V. After methanol injection at about 150 s, it is obvious that the chronoamperometric response of the Pt/C catalyst changes dramatically in terms of current density jumping from −0.1 mA cm^{-2} to 0.28 mA cm^{-2}, meaning that the sign of current changes from negative for the ORR to positive for the methanol oxidation reaction, an indication of susceptibility to methanol crossover. However, for NG catalyst, the chronoamperometric response of the NG catalyst recovers quickly after a violent fluctuation at the methanol injection, meaning that the catalyst possesses strong tolerance to the methanol crosses over from anode. It clearly demonstrates that our catalyst has superior tolerance against methanol crossover effect than Pt/C catalyst.

4. Conclusion

A high performance nitrogen-doped graphene catalyst has been prepared by a transfer pyrolysis and transfer nitrogen-doping approach, in which the graphene oxide was deoxidized and doped by the polyaniline put under the GO sample. The catalyst shows excellent activity toward the ORR with onset potential, half-wave potential and limiting current density comparable to those of commercial Pt/C catalyst in alkaline solution. It is revealed that the oxygen reduction on the catalyst follows a four-electron pathway, and the catalyst shows superior tolerance to the methanol, which generally crosses over from anode area of direct methanol fuel cells (DMFCs).

Acknowledgments

This work was financially supported by the National Scientific Foundation of China (NSFC Project Nos. 21076089, 20876062, 20673040), and Doctoral Fund of Ministry of Education of China (20110172110012). We would like to thank Professor Can Li at the Dalian Institute of Chemical Physics, Chinese Academy of Sciences, for the XPS characterization.

References

[1] S. Zhang, Y. Li, N. Pan, Journal of Power Sources 206 (2012) 476–482.
[2] X. Cao, Y. Shi, W. Shi, G. Lu, X. Huang, Q. Yan, Q. Zhang, H. Zhang, Small 7 (2011) 3163–3168.
[3] S. Yang, X. Feng, K. Müllen, Advanced Materials 23 (2011) 3575–3579.
[4] Z. Qin, Z.J. Li, M. Zhang, B.C. Yang, R.A. Outlaw, Journal of Power Sources 217 (2012) 303–308.
[5] Y.-C. Cao, C. Xu, X. Wu, X. Wang, L. Xing, K. Scott, Journal of Power Sources 196 (2011) 8377–8382.
[6] Y. Zhao, C. Hu, Y. Hu, H. Cheng, G. Shi, L. Qu, Angewandte Chemie International Edition 51 (2012) 11371–11375.
[7] S. Guo, S. Zhang, L. Wu, S. Sun, Angewandte Chemie International Edition 51 (2012) 11770–11773.
[8] L. Xiao, J. Damien, J. Luo, H.D. Jang, J. Huang, Z. He, Journal of Power Sources 208 (2012) 187–192.
[9] Y. Zhang, G. Mo, X. Li, J. Ye, Journal of Power Sources 197 (2012) 93–96.
[10] J. Hou, Z. Liu, P. Zhang, Journal of Power Sources 224 (2013) 139–144.
[11] C.-L. Liu, K.-H. Chang, C.-C. Hu, W.-C. Wen, Journal of Power Sources 217 (2012) 184–192.
[12] D. Zhang, X. Zhang, Y. Chen, P. Yu, C. Wang, Y. Ma, Journal of Power Sources 196 (2011) 5990–5996.
[13] S.D. Perera, R.G. Mariano, N. Nijem, Y. Chabal, J.P. Ferraris, K.J. Balkus Jr., Journal of Power Sources 215 (2012) 1–10.
[14] J.C. Meier, C. Galeano, I. Katsounaros, A.A. Topalov, A. Kostka, F. Schüth, K.J.J. Mayrhofer, ACS Catalysis 2 (2012) 832–843.
[15] K.E. Swider-Lyons, S.A. Campbell, The Journal of Physical Chemistry Letters 4 (2013) 393–401.
[16] J.X. Wang, H. Inada, L. Wu, Y. Zhu, Y. Choi, P. Liu, W.-P. Zhou, R.R. Adzic, Journal of American Chemical Society 131 (2009) 17298–17302.
[17] B. Lim, M. Jiang, P.H.C. Camargo, E.C. Cho, J. Tao, X. Lu, Y. Zhu, Y. Xia, Science 324 (2009) 1302–1305.
[18] Z. Chen, D. Higgins, A. Yu, L. Zhang, J. Zhang, Energy & Environmental Science 4 (2011) 3167–3192.
[19] M. Lefevre, E. Proietti, F. Jaouen, J.-P. Dodelet, Science 324 (2009) 71–74.
[20] S. Li, Y. Hu, Q. Xu, J. Sun, B. Hou, Y. Zhang, Journal of Power Sources 213 (2012) 265–269.
[21] M.S. Ahmed, S. Jeon, Journal of Power Sources 218 (2012) 168–173.
[22] J. Wu, Y. Wang, D. Zhang, B. Hou, Journal of Power Sources 196 (2011) 1141–1144.
[23] K. Gong, F. Du, Z. Xia, M. Durstock, L. Dai, Science 323 (2009) 760–764.
[24] X. Li, B.N. Popov, T. Kawahara, H. Yanagi, Journal of Power Sources 196 (2011) 1717–1722.
[25] X. Li, G. Liu, B.N. Popov, Journal of Power Sources 195 (2010) 6373–6378.
[26] N.P. Subramanian, X. Li, V. Nallathambi, S.P. Kumaraguru, H. Colon-Mercado, G. Wu, J.W. Lee, B.N. Popov, Journal of Power Sources 188 (2009) 38–44.
[27] V. Nallathambi, J.W. Lee, S.P. Kumaraguru, G. Wu, B.N. Popov, Journal of Power Sources 183 (2008) 34–42.
[28] H. Wang, Y. Liang, Y. Li, H. Dai, Angewandte Chemie 123 (2011) 11161–11164.
[29] G. Wu, N.H. Mack, W. Gao, S. Ma, R. Zhong, J. Han, J.K. Baldwin, P. Zelenay, ACS Nano 6 (2012) 9764–9776.
[30] J. Wu, D. Zhang, Y. Wang, Y. Wan, B. Hou, Journal of Power Sources 198 (2012) 122–126.
[31] Q. Wen, S. Wang, J. Yan, L. Cong, Z. Pan, Y. Ren, Z. Fan, Journal of Power Sources 216 (2012) 187–191.
[32] S. Yang, X. Feng, X. Wang, K. Müllen, Angewandte Chemie International Edition 50 (2011) 5339–5343.
[33] Z. Wang, R. Jia, J. Zheng, J. Zhao, L. Li, J. Song, Z. Zhu, ACS Nano 5 (2011) 1677–1684.
[34] Y. Liang, H. Wang, J. Zhou, Y. Li, J. Wang, T. Regier, H. Dai, Journal of American Chemical Society 134 (2012) 3517–3523.
[35] Y. Liang, Y. Li, H. Wang, J. Zhou, J. Wang, T. Regier, H. Dai, Nature Materials 10 (2011) 780–786.
[36] Z. Lin, G. Waller, Y. Liu, M. Liu, C.-P. Wong, Advanced Energy Materials 2 (2012) 884–888.

[37] S. Wang, L. Zhang, Z. Xia, A. Roy, D.W. Chang, J.-B. Baek, L. Dai, Angewandte Chemie International Edition 51 (2012) 4209–4212.
[38] J. Liang, Y. Jiao, M. Jaroniec, S.Z. Qiao, Angewandte Chemie International Edition 51 (2012) 11640–11641.
[39] S. Yang, L. Zhi, K. Tang, X. Feng, J. Maier, K. Müllen, Advanced Functional Materials 22 (2012) 3634–3640.
[40] R. Jiang, D.T. Tran, J. McClure, D. Chu, Electrochemistry Communications 19 (2012) 73–76.
[41] G. Wu, K.L. More, C.M. Johnston, P. Zelenay, Science 332 (2011) 443–447.
[42] G. Wu, M. Nelson, S. Ma, H. Meng, G. Cui, P.K. Shen, Carbon 49 (2011) 3972–3982.
[43] G. Wu, C.M. Johnston, N.H. Mack, K. Artyushkova, M. Ferrandon, M. Nelson, J.S. Lezama-Pacheco, S.D. Conradson, K.L. More, D.J. Myers, P. Zelenay, Journal of Materials Chemistry 21 (2011) 11392–11405.
[44] Y. Hu, X. Zhao, Y. Huang, Q. Li, N.J. Bjerrum, C. Liu, W. Xing, Journal of Power Sources 225 (2013) 129–136.
[45] Z. Mo, H. Peng, H. Liang, S. Liao, Electrochimica Acta 99 (2013) 30–37.
[46] R.N. Singh, R. Awasthi, Catalysis Science & Technology 1 (2011) 778–783.
[47] Y. Boudeville, F. Figueras, M. Forissier, J.-L. Portefaix, J.C. Vedrine, Journal of Catalysis 58 (1979) 52–60.
[48] J.H. Scofield, Journal of Electron Spectroscopy and Related Phenomena 8 (1976) 129–137.
[49] M. Jahan, Q. Bao, K.P. Loh, Journal of American Chemical Society 134 (2012) 6707–6713.
[50] I.-Y. Jeon, H.-J. Choi, S.-M. Jung, J.-M. Seo, M.-J. Kim, L. Dai, J.-B. Baek, Journal of American Chemical Society 135 (2012) 1386–1393.
[51] B. Zhao, P. Liu, Y. Jiang, D. Pan, H. Tao, J. Song, T. Fang, W. Xu, Journal of Power Sources 198 (2012) 423–427.
[52] Q. Shi, S. Mu, Journal of Power Sources 203 (2012) 48–56.
[53] H.R. Byon, J. Suntivich, Y. Shao-Horn, Chemistry of Materials 23 (2011) 3421–3428.
[54] F. Chen, P. Liu, Q. Zhao, Electrochimica Acta 76 (2012) 62–68.
[55] J. Liang, Y. Zheng, J. Chen, J. Liu, D. Hulicova-Jurcakova, M. Jaroniec, S.Z. Qiao, Angewandte Chemie International Edition 51 (2012) 3892–3896.
[56] B.F. Machado, P. Serp, Catalysis Science & Technology 2 (2012) 54–75.
[57] M. Zhong, E.K. Kim, J.P. McGann, S.-E. Chun, J.F. Whitacre, M. Jaroniec, K. Matyjaszewski, T. Kowalewski, Journal of American Chemical Society 134 (2012) 14846–14857.
[58] D.H. Lee, W.J. Lee, W.J. Lee, S.O. Kim, Y.-H. Kim, Physical Review Letters 106 (2011) 175502.
[59] Z. Chen, D. Higgins, Z. Chen, Carbon 48 (2010) 3057–3065.
[60] Z.-W. Liu, F. Peng, H.-J. Wang, H. Yu, W.-X. Zheng, J. Yang, Angewandte Chemie 123 (2011) 3315–3319.